Journal of Materials Chemistry A

Accepted Manuscript

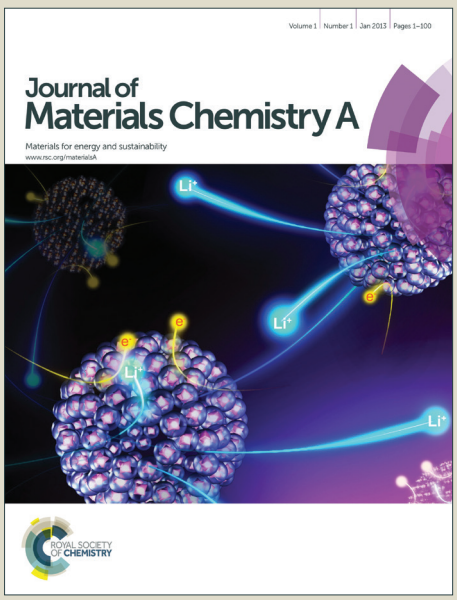

ROYAL SOCIETY OF CHEMISTRY

www.rsc.org/materialsA

Journal Name

RSCPublishing

ARTICLE

Single-Crystal $CoSe_2$ Nanorods as Efficient Electrocatalyst for Dye-Sensitized Solar Cells

Cite this: DOI: 10.1039/x0xx00000x

Hong Sun,[a] Lu Zhang[a] and Zhong-Sheng Wang[a]

Received 00th January 2012,
Accepted 00th January 2012

DOI: 10.1039/x0xx00000x

www.rsc.org/

Single-crystal $CoSe_2$ nanorods have been prepared with a facile one-step hydrothermal method. The thin $CoSe_2$ films fabricated by drop-casting the $CoSe_2$ nanorods suspension onto conductive substrates followed by simple drying without sintering can be used as highly efficient electrocatalyst for the reduction of I_3^-. The dye-sensitized solar cell (DSSC) with the standard N719 dye and the single-crystal $CoSe_2$ nanorod cathode achieves power conversion efficiency of 10.20% under AM1.5G one-sun illumination versus 8.17% for the Pt cathode. This finding implies that single-crystal $CoSe_2$ nanorod is a promising low-cost and high-performance cathode material for high-performance DSSCs.

Introduction

Since the seminal paper published by O'Regan and Grätzel in 1991,[1] dye-sensitized solar cells (DSSCs) have attracted tremendous interest in scientific research and industrial applications in the past two decades.[2] As one of the most promising photovoltaic devices, DSSCs have several advantages over silicon based solar cells such as ease of fabrication and cost-effectiveness. A typical DSSC is constructed with a working electrode (a dye-sensitized nanocrystalline TiO_2 film), a counter electrode (CE) and a redox-couple based electrolyte sandwiched between the two electrodes. The CE functions as an electrocatalyst to catalyze the reduction of I_3^- for effective circuit completion. Platinum (Pt) is so far the most commonly used CE for laboratory research due to its excellent electrocatalytic activity and chemical stability. Unfortunately, the high price and low abundance ratio of Pt create a big obstacle for large-scale application of DSSCs.[3] Therefore development of cheap CE materials with high electrocatalytic activity is of significance for practical applications.

A lot of alternatives to Pt have been developed for use as CE in DSSCs. The reported CE materials include carbon,[4] graphene,[5] conductive polymer[6] and metal compounds such as oxide,[7] sulfide,[8] nitride,[9] carbide,[10] and selenide.[11] Among them, metal selenides have drawn great attention due to their distinctive electronic properties, interesting chemical behaviours, and wide variety of potential applications.

Recently, $CoSe_2$ has drawn much attention and several synthetic methods have been reported in the literature.[12-14] We report herein single-crystal $CoSe_2$ nanorods for application as the CE in DSSCs. Excitingly, the single-crystal $CoSe_2$ nanorods exhibit excellent activity on the reduction of triiodide, and the DSSC with the single-crystal $CoSe_2$ nanorods CE produces a power conversion efficiency of 10.20% versus 8.17% for the Pt CE under the same conditions.

Results and discussion

Figure 1 shows the XRD pattern for the $CoSe_2$ powder sample. All the XRD diffraction peaks can be well indexed to orthorhombic $CoSe_2$ (JCPDS No. 00-053-0449). No other peaks of impurities are observed, indicating good purity of the synthesized samples. As compared to the ultrathin-layered $CoSe_2$ nanobelts,[12] which exhibited Bragg peaks in the small angle region due to the lamellar structure, the $CoSe_2$ sample prepared in this work did not show XRD peaks below 20^o of 2θ. The atomic ratio of Co:Se in the sample determined by EDS is 1.0:2.1, which is close to the stoichiometric ratio of $CoSe_2$. The atomic ratio of Co:Se in the sample determined by ICE-AES is 1.0:2.2, which is also close to the stoichiometric ratio of $CoSe_2$.

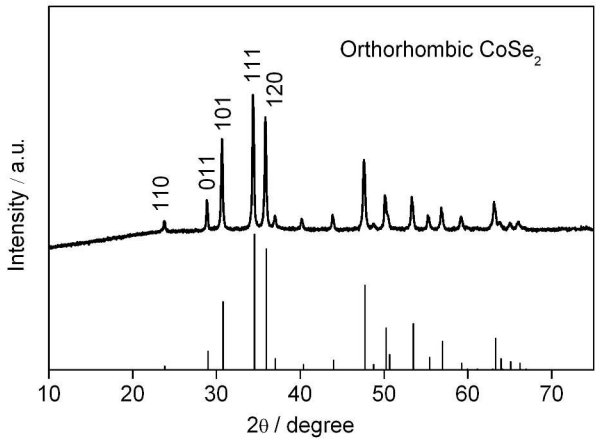

Figure 1. XRD pattern of the as-prepared $CoSe_2$ sample

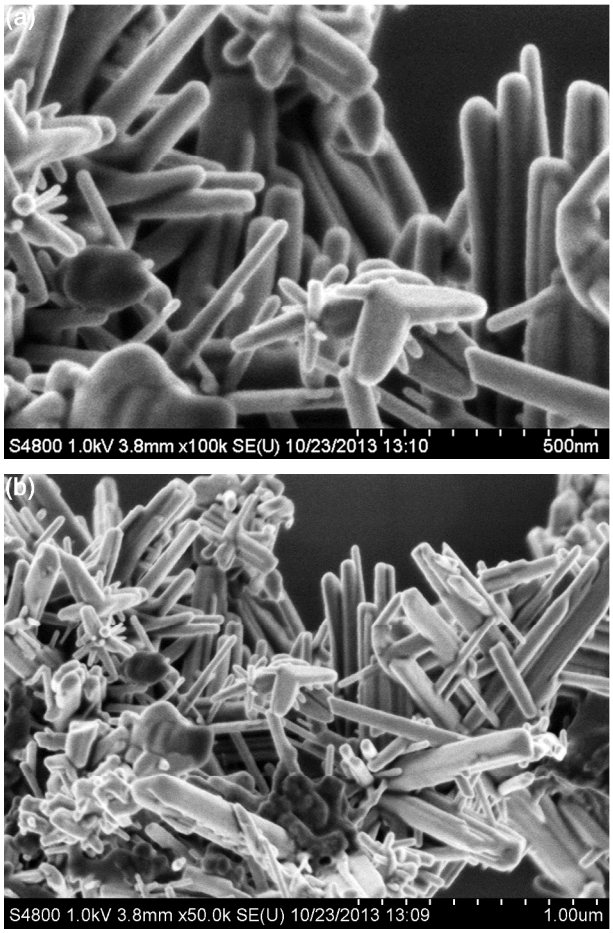

Figure 2. SEM images of the as-prepared $CoSe_2$ sample with different magnifications

Figure 2 displayed the SEM image of the as-prepared sample. $CoSe_2$ nanorods were formed after the hydrothermal reaction, as seen in the SEM images. The nanorods had broad distribution in size: 50-800 nm in length and 20-150 nm in width. The nanorod morphology was further confirmed with the TEM images (Figure 3a and 3b). The HRTEM image (Figure 3c) showed that the lattice spacing was 3.71 ± 0.01 Å, corresponding to the (110) planes of orthorhombic $CoSe_2$ (Figure 1). The selected area electron diffraction (SAED) spots shown in Figure 3d indicated the single crystalline nature of this nanorod. The electron diffraction pattern for the orthorhombic $CoSe_2$ nanorods is different from that for the layered $CoSe_2$ nanobelt.[12]

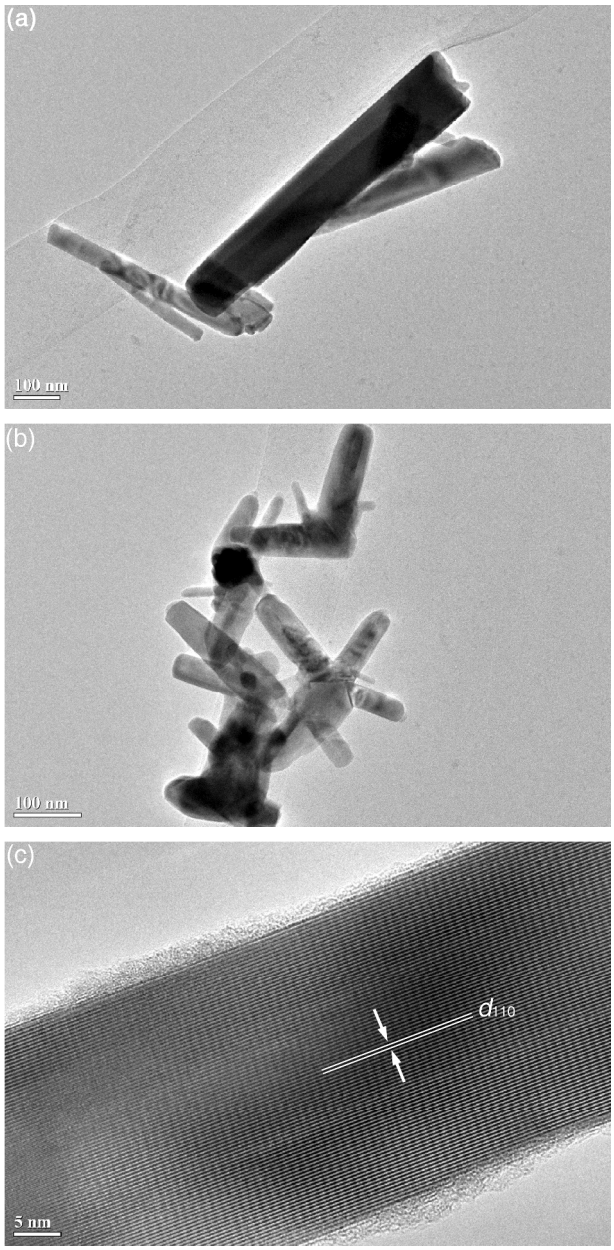

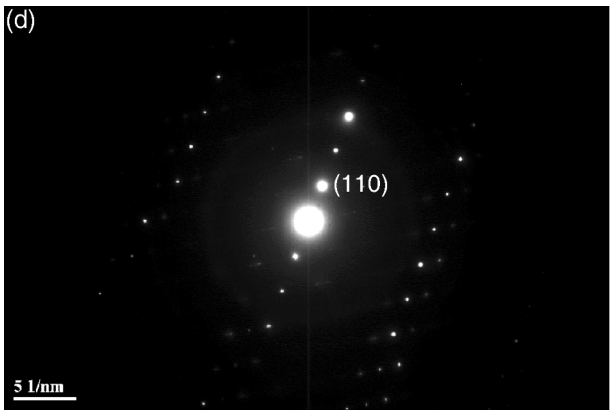

Figure 3. TEM images (a, b), HRTEM image (c) and SAED pattern (d) of the as-prepared $CoSe_2$ sample

$CoSe_2$ thin films are fabricated by drop-casting the $CoSe_2$ suspension onto FTO substrates. Figure 4 shows the SEM images of the $CoSe_2$ film. It is evident that the nanorods are deposited on the FTO surface, but the nanorods do not cover the surface completely. For comparison, the SEM image of the Pt deposited FTO is shown in Figure S1.

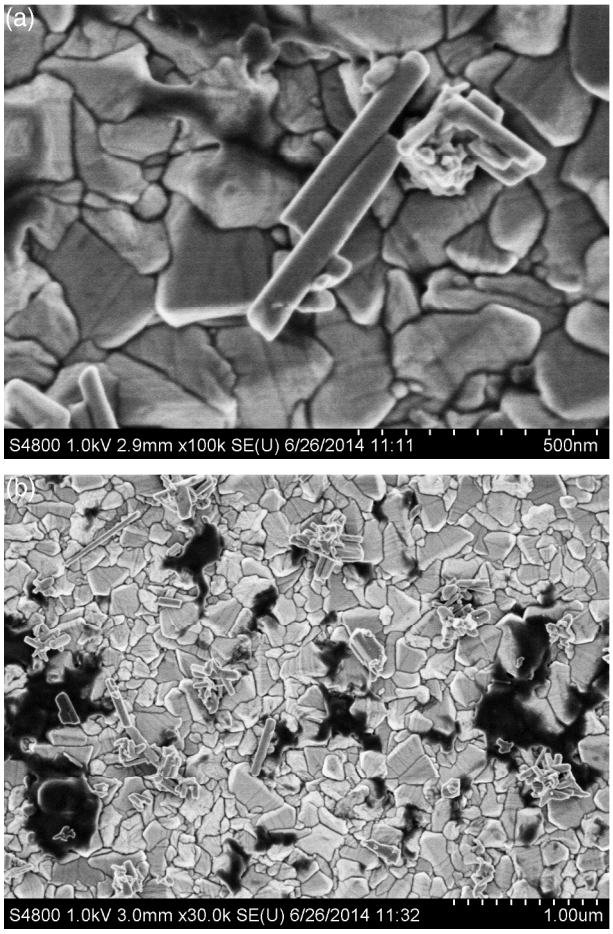

Figure 4. SEM images of the $CoSe_2$ film (loading amount of 20 μg cm^{-2})

Solar cell performance was optimized through varying the loading amount from 10 to 80 μg cm^{-2}. The efficiency increased with increasing the loading amount up to 20 μg cm^{-2}, and then decreased gradually with further increasing the loading amount. Therefore, the optimal loading was determined of 20 μg cm^{-2}, which was used for the fabrication of DSSCs and corresponding characterizations Three parallel DSSCs with each CE were constructed and tested under AM1.5G illumination (100 mW cm^{-2}) with a standard deviation error of 0.3% in absolute efficiency. Figure 5a displayed the photocurrent density-voltage (*J-V*) curve for the DSSC with the $CoSe_2$ CE and N719 dye. Impressively, the single-crystal $CoSe_2$ CE produced PCE of 10.20% with short-circuit photocurrent density (J_{sc}) = 18.55 mA cm^{-2}, open-circuit photovoltage (V_{oc}) = 753 mV and fill factor (FF) = 0.73. For comparison, the DSSC with the standard Pt CE was fabricated and measured at the same conditions. According to the *J-V* curve shown in Figure 5a, the Pt CE generated J_{sc} = 15.89 mA cm^{-2}, V_{oc} = 724 mV, FF = 0.71, corresponding to PCE of 8.17%. Evidently, replacement of the Pt CE with the single-crystal $CoSe_2$ nanorods CE causes a large increase in PCE by 25%, which is attributed to the significant improvement of J_{sc} and small increases in V_{oc} and FF.

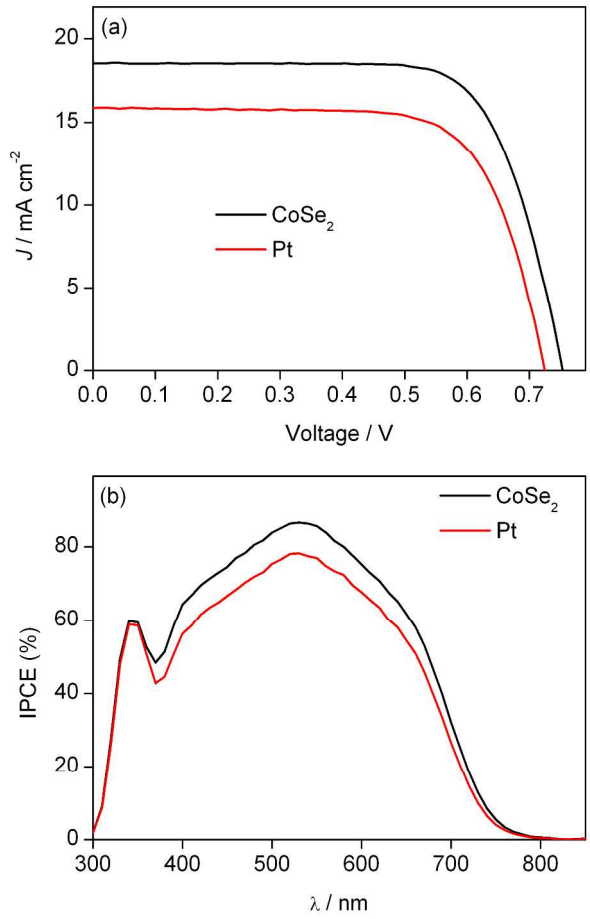

Figure 5. *J-V* curves (a) and IPCE spectra (b) of DSSCs with $CoSe_2$ and Pt CE, respectively

Figure 5b displays the IPCE spectra for the two DSSCs. The IPCE value for the $CoSe_2$ cathode is larger than that for the Pt

CE at each wavelength in the visible region. This accounts for the larger J_{sc} of the $CoSe_2$-based DSSC as compared to the Pt-based DSSC.

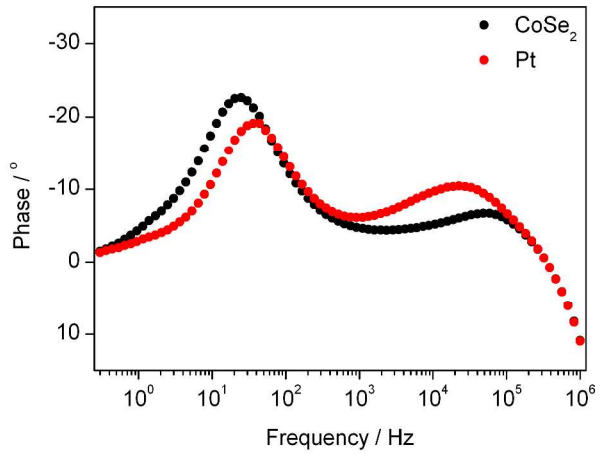

Figure 6. EIS Bode plots for the $CoSe_2$- and Pt-based DSSCs under one-sun illumination at open circuit

Although the anode and electrolyte are the same, the V_{oc} is different for the two DSSCs. For the same anode and electrolyte, the different cathode likely causes the difference of V_{oc}, which is determined by the photo-induced current and electron lifetime. To clarify this issue, electrochemical impedance spectroscopy (EIS) was measured. Figure 6 shows the EIS Bode plots for the two DSSCs. The left middle-frequency peak is attributed to charge recombination at the TiO_2/electrolyte interface. As compared to the Pt-based DSSC, this peak shifts to lower frequency for the $CoSe_2$-based DSSC, indicating a higher electron lifetime. The higher electron lifetime in combination with the higher J_{sc} for the $CoSe_2$-based DSSC is responsible for the higher V_{oc} as compared with the Pt-based DSSC.

The long-term stability of the DSSCs was evaluated by measuring the photovoltaic performance for eight days. The J_{sc} first decreased and then remained almost unchanged, while V_{oc}, FF and *PCE* first increased and then remained almost unchanged for the $CoSe_2$-based DSSC (Figure S2). By contrast, the J_{sc} first increased and then decreased, V_{oc} first increased followed by a plateau, FF remained stable for one day followed by a decrease, and *PCE* first increased followed by a slight decrease (5%) for the Pt-based DSSC. It seemed that the $CoSe_2$-based DSSC had better stability than the Pt-based DSSC under daylight storage.

As the DSSCs studied in this work are same in photoanode and electrolyte but different in CE, the solar cell performance should be related to the catalytic activity of the CE film. To interpret the difference of solar cell performance, electrocatalytic performances of four parallel electrodes for each sample were evaluated by measuring cyclic voltammograms (CV), electrochemical impedance spectra (EIS), and Tafel polarization. The relative standard deviation error was less than 5%. Figure 7 compares the CV curves of iodide/triiodide redox species on $CoSe_2$ and Pt electrodes, respectively. Two typical pairs of oxidation and reduction peaks (Ox-1/Red-1, Ox-2/Red-2, as labeled in Figure 7) are well resolved in the range of -0.6 to 0.9 V (*vs*. Ag/Ag^+) for both materials, similar to what has been reported for the DSSC systems in the literature.[11,15] According to the literature,[16-18] the Red-1 peak is attributed to the reduction of I_3^- to I^- while the Ox-1 peak is attributed to the oxidation of I^- to I_3^-. The Ox-2 peak is attributed to the oxidation of I_3^- to I_2 while the Red-2 peak is attributed to the reduction of I_2 to I_3^-. The characteristics of peaks Ox-1 and Red-1 are at the focus of our analysis because the CE of a DSSC is responsible for catalyzing the reduction of I_3^- to I^-. The peak-to-peak potential separation (E_{pp}) for the pair peaks is inversely correlated with the standard rate constant of a redox reaction. The E_{pp} is 0.36 and 0.44 V for $CoSe_2$ and Pt, respectively. This indicates that the reduction rate constant of triiodide to iodide on the single-crystal $CoSe_2$ nanorod is faster than on the Pt electrode. In addition, the $CoSe_2$ nanorod exhibits higher peak currents than the Pt electrode. It is thus concluded that the single-crystal $CoSe_2$ nanorod has higher electrocatalytic performance than the Pt on the reduction of triiodide due to the larger reduction rate constant and higher redox peak currents.

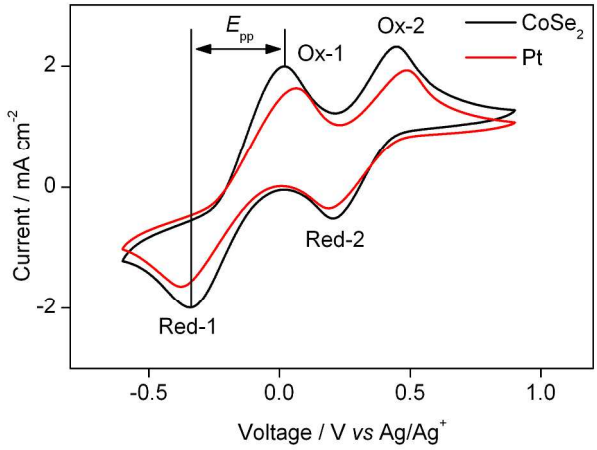

Figure 7. CV curves of iodide/triiodide redox species on $CoSe_2$ and Pt electrodes, respectively. The current is normalized to geometric area.

To further elucidate the catalytic performance, electrochemical impedance spectroscopy (EIS) was recorded with a symmetric dummy cell, in which a thin layer of redox electrolyte solution used in the DSSC was sandwiched between two identical electrodes (CE/electrolyte/CE). Figure 8a shows the EIS Nyquist plots where two semicircles were observed. As small amount of catalyst was deposited on FTO, electrolyte diffusion in catalyst pores was not observed.[5] According to the Randles-type circuit (inset of Figure 8a),[19] the high-frequency intercept on the real axis represents the series resistance (R_s). The left arc arises from the charge-transfer resistance (R_{ct}) at the electrode/electrolyte interface and the corresponding constant phase angle element (CPE), which describes the deviation from ideal capacitance due to the roughness of the electrode.[19] The right semicircle reflects the Nernst diffusion impedance (Z_N) of the I^-/I_3^- redox couple in the electrolyte. R_{ct}

determined by fitting the impedance spectra using the Z-view software is 2.0 and 3.0 Ω for $CoSe_2$ and Pt, respectively. As the apparent surface area is 0.70 and 0.48 cm^2 for $CoSe_2$ and Pt, respectively, estimated from the product of loading amount, geometric area (0.36 cm^2) of the CE and BET surface area, the normalized R_{ct} is 1.4 Ω cm^2 for both electrodes. Since R_{ct} correlates inversely with the electrocatalytic performance, $CoSe_2$ and Pt CE films have comparable catalytic activity taking the apparent surface area into account, but the former exhibits higher electrocatalytic performance than the latter due to the larger apparent surface area.

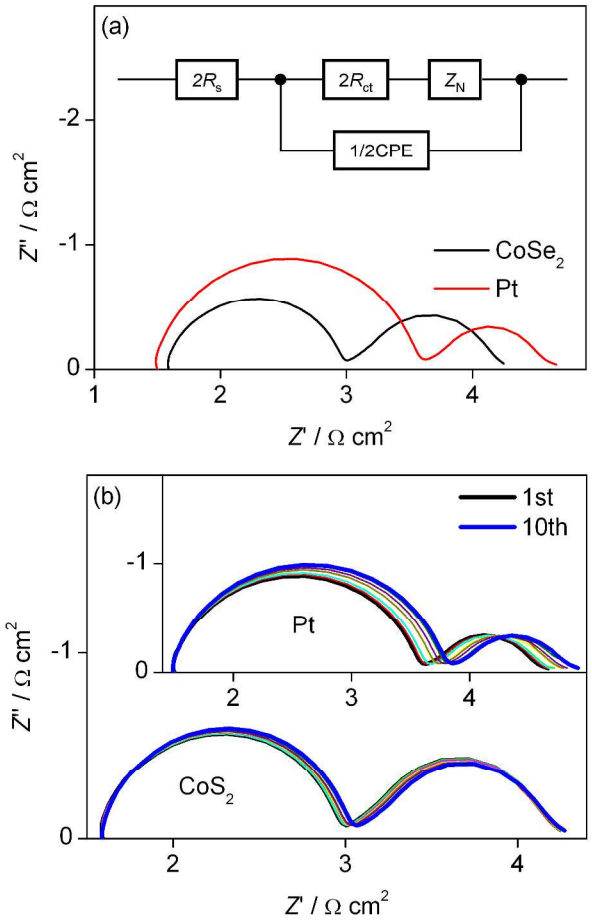

Figure 8. EIS Nyquist plots for symmetric cells fabricated with $CoSe_2$, and Pt electrodes, respectively (a). The inset in (a) gives the equivalent circuit. Evolution of EIS for the dummy cells (b). The cell was first subjected to CV scanning from 0 to 1 V, then to -1 V and finally to 0 V with a scan rate of 100 mV s^{-1} followed by 20 s relaxation at 0 V, and then EIS was recorded. This sequential test was repeated for ten cycles.

The Z_N for the $CoSe_2$ CE (3.4 Ω or 2.4 Ω cm^2 normalized to the apparent area) is larger than that for the Pt CE (1.2 Ω or 0.6 Ω cm^2 normalized to the apparent surface area). The Z_N describes the impedance of electrolyte diffusion: [19]

$$Z_N = \frac{kT}{n^2 e_0^2 c(I_3^-) A \sqrt{D(I_3^-) i\omega}} \tanh\left(\sqrt{\frac{i\omega}{D(I_3^-)}}\delta\right) \quad (1)$$

where k is the Boltzmann constant, T is the temperature, n is the number of electrons involved in the reduction of I_3^- at the electrode, e_0 is the elementary charge, $c(I_3^-)$ is the concentration of I_3^-, ω is the angular frequency, $D(I_3^-)$ is the diffusion constant, A is the electrode area, and δ is the diffusion layer thickness (half the distance between electrodes in the dummy cell). As Z_N is inversely proportional to the concentration of I_3^-, the larger Z_N for the $CoSe_2$ electrode indicates a lower concentration of I_3^-. However, the initial concentration of I_3^- is same for both dummy cells. It is thus speculated that the concentration of I_3^- has changed in the dummy cell, which may be influenced by the adsorption of I_3^- on the electrode. To probe this possible change, we measured the adsorption of I_3^- on $CoSe_2$ and Pt by means of UV-vis absorption spectra (Figure S3). It is clearly seen from Figure S1 that more than 3-fold I_3^- is adsorbed on $CoSe_2$ as compared to the Pt film. Normalized to the apparent surface area, the I_3^- ions adsorbed on the $CoSe_2$ CE are about 2-fold that on the Pt CE. This means that the $CoSe_2$ has higher adsorption capacity for I_3^- ions than the Pt. Higher adsorption of I_3^- on the $CoSe_2$ CE signifies the reduction of concentration in the bulk, which reduces the electrolyte conductivity and thus increases the Z_N. However, the higher adsorption of I_3^- on the $CoSe_2$ CE is advantageous to fast reduction of I_3^-, which is at least partly responsible for its lower R_{ct} as compared to the Pt CE.

Figure 8b shows the evolution of impedance spectra for the dummy cells subjected to sequential scans of CV and EIS for 10 cycles. After 10 cycles of scanning, there was almost no change of R_s and Z_N, indicating that the potential cycling hardly influenced the series ohmic resistance and the mass transport in the redox solution. However, R_{ct} increased by 0.05 Ω for $CoSe_2$ and 0.3 Ω for Pt after 10 cycles of scanning. This indicates that $CoSe_2$ had better electrochemical stability than Pt, which is responsible for the better long-term stability of the $CoSe_2$-based DSSC as compared to the Pt-based DSSC.

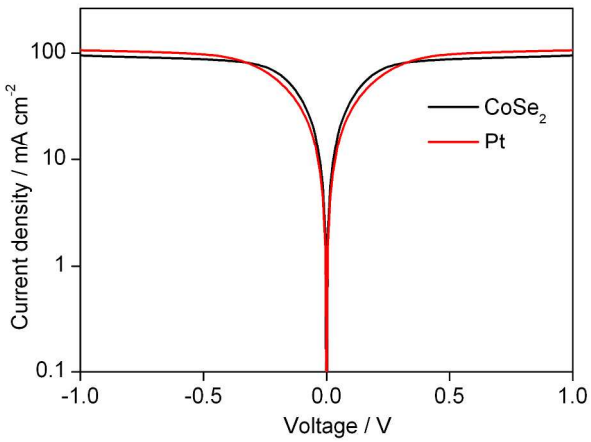

Figure 9. Tafel polarization curves for the dummy cells with $CoSe_2$ and Pt, respectively

Furthermore, Tafel polarization was carried out to disclose the information of diffusion-limited current and charge exchange at the CE/electrolyte interface. Figure 9 shows the

Tafel curves of the dummy cells, in which saturation currents (i.e. the limiting current density J_{lim}) were observed for both $CoSe_2$ and Pt based DSSCs. Owing to the large excess of I^- in the electrolyte, only the diffusion of I_3^- limits the current.[19] The J_{lim} is proportional to the diffusion constant ($D(I_3^-)$) and concentration ($c(I_3^-)$) of I_3^-.[19]

$$J_{lim} = \frac{2nFD(I_3^-)c(I_3^-)}{l} \quad (2)$$

where F is Faraday's constant, l is the distance between the electrodes in the dummy cell. The J_{lim} for Pt is larger than that for $CoSe_2$. This indicates that the concentration of I_3^- in the bulk is smaller for the $CoSe_2$ electrode, which is caused by the higher adsorption of I_3^- on the $CoSe_2$ electrode (Figure S1). The result for electrolyte diffusion obtained from the Tafel curve is consistent with that from the EIS analysis.

The charge exchange current density (J_0) can be estimated from the slope of the anodic or cathodic branch in the Tafel curve. It is seen from Figure 9 that the $CoSe_2$ electrode gives larger slope than the Pt electrode, indicating that the J_0 for the former is larger than that for the latter. J_0 can be also calculated from R_{ct} obtained from EIS measurement.[19]

$$J_0 = \frac{kT}{nFR_{ct}} \quad (3)$$

where R is the gas constant. As the R_{ct} (normalized to the geometric area) for the $CoSe_2$ electrode is smaller than that for the Pt, the J_0 for the former derived from equation (3) is larger than that for the latter, which is in good agreement with the result from Tafel curves.

The above results indicate that single-crystal $CoSe_2$ nanorods supersede Pt in terms of electrocatalytic performance. The higher electrocatalytic performance is responsible for the higher FF and J_{sc} for single-crystal $CoSe_2$ nanorods, as compared to the Pt CE. To avoid current losses at the CE, the J_0 should be sufficiently high.[20] In principle, high J_0 is favourable for high J_{sc}. The observed higher J_{sc} for the $CoSe_2$ CE is likely attributed to its higher J_0.[20]

Experimental

Synthesis of $CoSe_2$. The $CoSe_2$ nanorod was synthesized *via* a one-step hydrothermal reaction.[14] Briefly, 0.320 g Se powder (99.999%, Aladding) was dissolved in 30 ml of NaOH (4 g, Sinopharm) aqueous solution to form solution A. Solution B was prepared from 0.587 g $Co(NO_3)_2 \cdot 6H_2O$ (99.9%, Alfa Aesar) dissolved in 10 mL of 0.25 M EDTA-2Na (>99%, J&K). The two solutions were then added to a 100 mL Teflon-lined autoclave under stirring for several minutes. The autoclave was tightly sealed and heated at 200 ^oC for 6 h and then cooled down to RT naturally. A large amount of black precipitate was collected, which was washed with dilute acid and distilled water for several cycles followed by drying at 60 ^oC for 24 h.

Fabrication and Evaluation of DSSCs. 1.8 mg of $CoSe_2$ nanorods was dispersed in 10 mL of distilled water and ethanol (volume ratio, 1:1) by ultrasonication for 1 h. The $CoSe_2$ suspensions were drop-casted on conductive glass (fluorine-doped SnO_2, FTO, 15 Ω/square, transmittance 85%, Nippon Sheet Glass Co., Ltd., Japan), which was masked by a 3M Scotch tape with an exposed area of 0.6 × 0.6 cm^2. Then the films were dried in an oven at 70 °C. As a reference, pyrolytic Pt CE was prepared by drop-casting 50 μL of H_2PtCl_6 in ethanol (5 mM) on FTO glass followed by sintering at 380 °C for 30 min. TiO_2 films (18 μm thick) composed of transparent layer (12 μm, 25 nm TiO_2 nanoparticles) in contact with FTO and scattering layer (6 μm, 25 nm TiO_2 nanoparticles (60%) + 300 nm TiO_2 nanoparticles (40%)) on top of the transparent layer were prepared by a screen-printing method on FTO glass according to a previous report.[21] TiO_2 films were soaked overnight in cis-di(isothiocyanato)-bis-(2,2-bipyridyl-4,4-dicarboxylato)ruthenium (II) bis-tetrabutyl ammonium (so-called N719, used as received from Solaronix SA) solution (0.3 mM in a mixed solvent of acetonitrile and tert-butanol in a volume ratio of 1:1). The dye-sensitized TiO_2 photoanode and the CE were separated by a hot-melt Surlyn film (30 μm thick) and sealed through hot pressing. The electrolyte (0.1 M LiI, 0.05 M I_2, 0.6 M 1,2-dimethyl-3-n-propylimidazolium iodide, and 0.5 M 4-tert-butylpyridine in absolute acetonitrile) was injected into the interspace between the photoanode and CE. Finally, the holes on the back of the CE were sealed with a Surlyn film covered with a thin glass slide under heat.

Characterizations. X-ray diffraction (XRD) profile was recorded on an X-ray powder diffractometer (D8 Advance, Bruker) with Cu Kα radiation (λ= 0.154 nm). The morphology and atomic ratio of the selenide sample were examined by field emission scanning electron microscopy (FESEM, S-4800, Hitachi) with energy-dispersed spectroscopy (EDS). The composition of selenide was also detected by inductively coupled plasma-atomic emission spectrum (ICP-AES, Thermo Electron Corp. Adv. ER/S). The microstructure was characterized with high-resolution transmission electron microscopy (HRTEM, JEM-2100F, JEOL). The specific surface area was measured with a Micromeritics ASAP2020 nitrogen adsorption-desorption apparatus. Cyclic voltammetry (CV) was carried out in a three-electrode system containing an anhydrous acetonitrile solution of 0.1 M $LiClO_4$, 10 mM LiI, and 1 mM I_2 at a scan rate of 50 mV s^{-1}, using a Pt wire as the CE, an Ag/Ag^+ electrode as the reference electrode, and the as-prepared $CoSe_2$ film as the working electrode. Electrochemical impedance spectroscopy (EIS) and Tafel polarization measurements were performed on the symmetrical dummy cells assembled with two identical electrodes filled with the same electrolyte as used in the DSSC. The active geometric area of the dummy cell was 0.36 cm^2 with a distance of 30 μm between the electrodes. In the EIS test, the dummy cell was scanned from 0.1 Hz to 800 kHz at 0 V bias and ac amplitude of 10 mV. The EIS of DSSCs was carried out on an electrochemical workstation at 0 V bias and ac amplitude of 10 mV, which includes a white light emitting diode and the corresponding control system. All the electrochemical characterizations were performed on an electrochemical workstation (ZAHNER

ZENNIUM CIMPS-1, Germany). The photocurrent density-voltage curves of DSSCs were recorded on a Keithley 2400 source meter under the illumination of AM1.5G simulated solar light coming from an AAA solar simulator (Newport-94043A) equipped with a Xe lamp (450 W) and an AM1.5G filter. The light intensity was calibrated using a reference Si solar cell (Oriel-91150). A black mask with an aperture area of 0.2304 cm^2 was applied on the surface of DSSCs to avoid stray light completely.

Conclusions

In summary, we have applied single-crystal $CoSe_2$ nanorods as the CE in DSSCs. $CoSe_2$ exhibits excellent electrocatalytic activity on the reduction of I_3^-, and the DSSC with the $CoSe_2$ CE produces higher power conversion efficiency (10.20%) than the DSSC with the Pt CE (8.17%). The results presented in this work imply that sing-crystal $CoSe_2$ nanorod is a promising low-cost and high-performance cathode material for application in DSSCs.

Acknowledgements

This work was financially supported by the National Basic Research Program (No. 2011CB933302) of China, STCSM (12JC1401500) and Jiangsu Major Program (BY2010147).

Notes and references

[a] Department of Chemistry, Lab of Advanced Materials, Collaborative Innovation Center of Chemistry for Energy Materials, Fudan University, 2205 Songhu Road, Shanghai 200438, P. R. China

* Corresponding author: E-mail: zs.wang@fudan.edu.cn, Fax/Tel: (+86)21-5163-0345.

† Footnotes should appear here. These might include comments relevant to but not central to the matter under discussion, limited experimental and spectral data, and crystallographic data.

Electronic Supplementary Information (ESI) available: The UV-vis absorption spectra of the electrode films before and after adsorbing I_3^- species. See DOI: 10.1039/b000000x/

1 B. O'Regan and M. Grätzel, *Nature* 1991, **353**, 737.
2 M. Grätzel, *Nature* **2001**, *414*, 338.
3 T. N. Murakami and M. Grätzel, *Inorg. Chim. Acta* 2008, **361**, 572.
4 K. Suzuki, M. Yamaguchi, M. Kumagai and S. Yanagida, *Chem. Lett.* 2003, **32**, 28.
5 L. Kavan, J. H. Yum and M. Grätzel, *Nano Lett.* 2011, **11**, 5501.
6 H. Wang, Q. Feng, F. Gong, Y. Li, G. Zhou and Z.-S. Wang, *J. Mater. Chem. A* 2013, **1**, 97.
7 J. Xia, C. Yuan and S. Yanagida, *ACS Appl. Mater. Interfaces* 2010, **2**, 2136.
8 (a) M. K. Wang, A. M. Anghel, B. Marsan, N. C. Ha, N. Pootrakulchote, S. M. Zakeeruddin and M. Grätzel, *J. Am. Chem. Soc.* 2009, **131**, 15976. (b) C.-W. Kung, H.-W. Chen, C.-Y. Lin, K.-C. Huang, R. Vittal, K.-C. Ho, *ACS Nano* 2012, **6**, 7016.
9 G. Li, J. Song, G. Pan and X. Gao, *Energy Environ. Sci.* 2011, **4**, 1680.
10 M. Wu, X. Lin, A. Hagfeldt and T. Ma, *Angew. Chem. Int. Ed*. 2011, **50**, 3520.
11 F. Gong, H. Wang, X. Xu, G. Zhou and Z.-S. Wang, *J. Am. Chem. Soc*. 2012, **134**, 10953.
12 M.-R. Gao, W.-T. Yao, H.-B. Yao, S.-H. Yu, *J. Am. Chem. Soc*. 2009, **131**, 7486.
13 I. A. Ji, H. M. Choi, J. H. Bang, Mater. Letter. 2014, **123**, 51.
14 W. Zhang, Z. Yang, J. Liu, Z. Hui, W. Yu, Y. Qian, G. Zhou and L. Yang, *Mater. Res. Bull.* 2000, **35**, 2403.
15 J. D. Roy-Mayhew, D. J. Bozym, C. Punckt and I. A. Aksay, *ACS Nano* 2010, **4**, 6203.
16 A. I. Popov and D. H. Geske, *J. Am. Chem. Soc*. 1958, **80**, 5346.
17 F. G. K. Baucke, R. Bertram and K. Cruse, *J. Electroanal. Chem*. 1971, **32**, 247.
18 G. Boschloo and A. Hagfeldt, *Acc. Chem. Res*. 2009, **42**, 1819.
19 A. Hauch and A. Georg, *Electrochim. Acta* 2001, **46**, 3457.
20 S. Ahmad, E. Guillén, L. Kavan, M. Grätzel, M. K. Nazeeruddin, *Energy Environ. Sci*. 2013, **6**, 3439.
21 Z.-S. Wang, H. Kawauchi, T. Kashima and H. Arakawa, *Coord. Chem. Rev*. 2004, **248**, 1381.